Role of π-d hybridization in a 300-K organic-magnetic interface: Metal-free phthalocyanine single molecules on a bcc Fe(001) whisker

T. K. Yamada,[1,2,*] Y. Yamagishi,[1] S. Nakashima,[1] Y. Kitaoka,[3] and K. Nakamura[4]

[1]*Graduate School of Advanced Integration Science, Chiba University, 1-33 Yayoi-cho, Inage-ku, Chiba 263-8522, Japan*

[2]*Molecular Chirality Research Center, Chiba University, 1-33 Yayoi-cho, Inage-ku, Chiba 263-8522, Japan*

[3]*National Institute of Advanced Industrial Science and Technology (AIST), Spintronics Research Center, 1-1-1 Umezono, Tsukuba, Ibaraki 305-8568, Japan*

[4]*Department of Physics Engineering, Mie University, 1577 Kurimamachiya-cho, Tsu City 514-8507, Mie, Japan*

(Received 3 February 2016; revised manuscript received 31 October 2016; published 28 November 2016)

The realization of single molecular electronics is considered the next frontier to addressing and sustaining the storage needs of the future. In order to realize a single molecular device working at 300 K, two conditions must be satisfied: first, there must be no molecular diffusion, i.e., robust bonding between molecules and the contacting electrode, and second, stable electronic interface states. In this study, using a combination of 7-K and 300-K ultrahigh vacuum scanning tunneling microscopy/spectroscopy experiments and theoretical *ab initio* calculations, we investigated the adsorption of π-conjugated metal-free phthalocyanine (Pc) single molecules onto an Fe(001) whisker single crystal along with the resulting electronic interface structures. The Pc/Fe(001) system was found to prevent molecular diffusion even at 300 K, due to strong adsorption as well as the presence of a larger diffusion barrier than that of the Pc/Ag(001) system, in which molecules are known to diffuse at 300 K. The origin of such a robust bonding was studied by recovering the sample local density of states (LDOS) with the normalized $(dI/dV)/T$ curves, where the LDOS peaks are successfully explained by theoretical calculations.

DOI: 10.1103/PhysRevB.94.195437

I. INTRODUCTION

The realization of single-molecule devices is considered the next frontier to addressing and sustaining the storage needs of the future. In order to realize a single-molecule junction working at 300 K, one condition must be satisfied: there must be robust bonding between molecules and the contacting electrode. The drastic increase in the use of computers and the internet has led to an increasing demand for high-capacity storage devices. Within current limitations in terms of resources and energy, nanotechnology and nanomaterials, which have aided in significantly reducing device sizes, have been considered as a key solution to building devices that can address the memory needs of the future. In this backdrop, researchers have focused on nanomaterials such as carbon nanotubes, graphene, and molecular films to realize compact and flexible electronic devices [1–8]. Single molecules with sizes less than 1 nm have attracted attention as potential nanomaterials for future electronic devices [9–38].

Single organic molecules adsorbed onto various electrodes have been studied using both scanning tunneling microscopy (STM) as well as STM break-junction approaches. Insulating electrodes such as MgO, NaCl, and CuN [9–11] are powerful templates to visualize intrinsic molecular highest occupied and lowest unoccupied molecular orbital (HOMO and LUMO, respectively) states. Electronic interactions determine the bonding strength between π-conjugated single organic molecules and substrate electrodes, i.e., the insulating electrode exhibits negligible electronic interaction with the substrate.

Metallic substrates, mainly noble metals such as Au, Ag, Cu, and Pt, are also frequently used to realize phenomena such as Kondo resonance [12–23]. It is well known that π-conjugated single molecules adsorbed onto noble metal electrodes such as fcc Au, Ag, Cu, or Pt diffuse and form a two-dimensional ordered film at 300 K [20,22–25]. Because the molecules move across the noble metal electrode surface, in break-junction measurements, the single molecule can "fit" between the two electrodes [32–38]. Noble metal surfaces, in which mainly s or p states are dominant near the Fermi energy (E_F), interact weakly with the molecule, essentially through the process of physisorption.

With metal-free single organic molecules supported by 3d magnetic metals such as Fe, Co, Cr, and Mn, giant magnetoresistance (GMR) junctions have been successfully realized in a spin-polarized STM; the GMR value thus achieved was +60% for [Co(111)/H_2Pc/Co(111)], −50% for [Mn(001)/H_2Pc/Fe(110)], and −30% for [Fe/C_{60}/Cr] single molecular junctions [14–16]. The interfaces between organic molecules and 3d magnets appear to be spin-polarized even without the presence of magnetic ions in molecules due to hybridization between the d and π states, and thus, the molecules are likely chemisorbed; consequently, the distance between the substrate and the molecule is less than that in the physisorption case due to the strong nature of chemisorbed bonds.

In this study, metal-free phthalocyanine (H_2Pc) single molecules are investigated as one of the ideal metal-free π-conjugated molecules by means of ultrahigh vacuum (UHV) scanning tunneling microscopy and spectroscopy (STM/STS) at 7 K and room temperature (RT). We focus on using a bcc Fe(001)-whisker single crystal as the substrate electrode since the procedure to obtain a uniform surface, distinct electronic spin structures, and clear magnetic domain patterns for this single crystal has been well studied [39–41]. Further, whiskers prepared via the chemical vapor deposition method contain extremely low concentrations of impurities when compared with those in commercial Fe single crystals. 0.1-ML H_2Pc molecules were adsorbed on the Fe(001) whisker at 300 K.

*Corresponding author: toyoyamada@faculty.chiba-u.jp

Different types of adsorption sites and new local density of state (LDOS) peaks were confirmed. *Ab initio* calculations identified the origin of the new interface state peaks, i.e., hybridization of molecular π and Fe(001) d states. Different LDOS inside single H_2Pc molecules are confirmed experimentally and theoretically. With a comparison of H_2Pc/Ag(001), where there is no hybridization of π-d states, H_2Pc molecules on Fe(001) were found to have a more than 3 times higher diffusion barrier and adsorption energy. Experimentally, H_2Pc molecules on Fe(001) did not diffuse and immobilize by STM manipulation, indicating worse knowledge to realize 300 K single molecular devices.

II. METHODS AND EXPERIMENTS

A. STM and spectroscopy measurements

STM experiments were performed at 7 K and 300 K in ultrahigh vacuum (UHV, base pressure $< 8 \times 10^{-9}$ Pa). One of the most effective techniques for precisely measuring the LDOS of 1-nm-size molecules is tunneling spectroscopy with an STM setup, which is known as scanning tunneling spectroscopy [24]. STS measurements were performed by opening the feedback loop of the tunneling current, i.e., fixing the tip-sample separation (z). The tunneling current was measured at each pixel by varying the sample voltage to obtain the $I(V)$ curves, where zero voltage corresponds to the Fermi energy. The differential conductivity (dI/dV) curves were obtained by numerical differentiation of the $I(V)$ curves. The LDOS was obtained by the normalization of dI/dV curves using the T background, i.e., $(dI/dV)/T$ below the Fermi energy indicates occupied LDOS and $(dI/dV)/T$ above the Fermi energy indicates unoccupied LDOS, where T denotes the fitted tunneling probability functions: $T = a\exp(-2z\sqrt{\phi - eV/2}) + b\exp(-2z\sqrt{\phi + eV/2})$, where a and b denote fitting parameters, ϕ the averaged barrier height between tip and sample, and z the tip-sample separation [24,42–45]. In this study, we used $\phi = 4.5$ eV and $z = 10$ Å, but we also tested the normalization with different ϕ (4.0−5.5 eV) and z (5−11 Å), while we always succeeded to recover the peaks at the same energy positions within ± 20 meV (see also Ref. [24]).

B. Sample and tip preparations

STM tungsten (W) tips were electrochemically etched from W wires ($\phi = 0.3$ mm, purity 99.9%) in air using aqueous KOH. The tip was rinsed with hot water and acetone and subsequently transferred into the load-lock chamber of our STM setup. The apex of the W tip was annealed to obtain an impurity-free apex under UHV conditions [46].

Fe-whisker single crystals were grown by using the chemical vapor deposition (CVD) technique to obtain high-purity Fe samples [39–41]. As shown in Fig. 1(a), the $FeCl_2$ powder was set in the quartz tube inside the furnace. By flowing H_2 gas into the tube at 750 °C, Fe whiskers were grown inside the tube [see Fig. 1(b)]. The scanning electron microscopy (SEM) image in Fig. 1(c) shows that one whisker has a rectangular shape with a 10–50 mm length and a 0.1–1-mm side. The x-ray Laue image in Fig. 1(d) confirmed that the our Fe whiskers have bcc (001) surfaces at the side planes. Magnetic imaging by SEM with

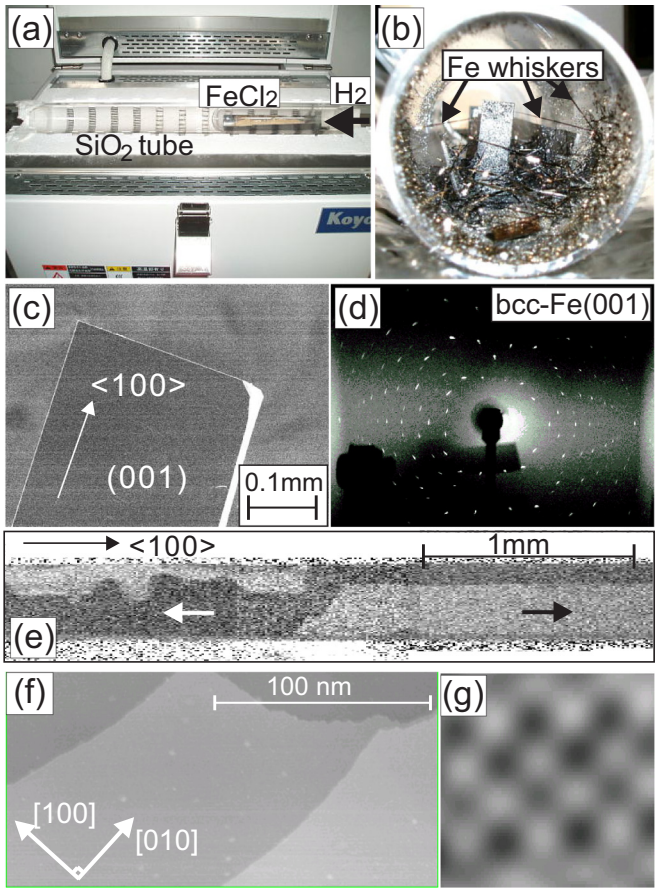

FIG. 1. (a) A picture of a furnace growing Fe whiskers from $FeCl_2$ powders with H_2 gas, chemical vapor deposition (CVD) process. (b) A picture of grown Fe whiskers inside the SiO_2 tube. (c) Scanning electron microscopy (SEM) image of the single Fe whisker. (d) X-ray Laue image obtained from the whisker. (e) Magnetic domain image by our homebuilt SEM with polarization analysis (SEMPA). (f) Scanning tunneling microscopy (STM) topographic images of the Fe(001) whisker surface (215 × 108 nm). (g) An atomically resolved STM image of Fe(001) (1.1 × 1.1 nm).

polarization analysis (SEMPA) showed magnetic domains of the Fe whisker. The typical size is 0.5 × 1.0 mm, and the easy axis is in the ⟨100⟩ direction (long axis). The whisker that was introduced from air into the UHV chamber was first cleaned by Ar^+ sputtering and flattened by annealing up to 870 K nearly two dozen times. Before STM measurements, the whisker was sputtered at 870 K for 30 min. The annealing was stopped 5 min after stopping the sputtering, which produced a clean and atomically flat Fe(001) surface. Figure 1(f) shows a topographic STM image of the Fe(001) whisker single crystal at room temperature in ultrahigh vacuum. Atomic terraces larger than 100 nm are observed. The atomically resolved STM image in Fig. 1(g) indicates the presence of bcc (001) symmetry.

Commercial metal-free π-conjugated phthalocyanine (H_2Pc) powder (Alfa Aesar, purity 95%) was purified by sublimation at 653 K and recrystallization at 473 K under a pressure of 10^{-3} Pa (yield 30%). NMR and infrared spectra of the samples were used to confirm the absence of impurities after purification. The clean H_2Pc powder was placed in a

crucible, which was set in a molecular chamber and heated to 550 K. H_2Pc molecules were deposited on the Fe(001) whisker in a UHV preparation chamber and subsequently transferred to an analytical STM chamber under UHV.

C. *Ab initio* calculations

Calculations were carried out based on the generalized gradient approximation (GGA) [47] by using the full-potential linearized augmented plane-wave (FLAPW) method with single-slab geometry [48–50]. LAPW basis sets with cutoffs of $|k+G| \leqslant 3.6$ a.u.$^{-1}$ and muffin-tin (MT) sphere radii of 2.2 a.u. for Ag and Fe, 1.2 a.u. for N and C, and 0.8 a.u. for H were used; lattice harmonics with angular momenta up to $l = 8$ for Ag and Fe, 6 for N and C, and 4 for H were employed to expand the charge and spin densities. As a model, we adopted a single H_2Pc molecule on a three-layer Ag(001) [and Fe(001)] slab with four different adsorption sites, wherein the center of the molecule locates at the hollow, top (T), and saddle (B1 and B2) sites on the substrate surface. The in-plane bulk lattice constants of Ag and Fe were assumed, and the atomic positions of H_2Pc and the substrate up to the second layer from the surface were fully optimized by atomic force calculations, while the layer–layer distance on the opposite side was fixed to the corresponding bulk values.

III. RESULTS AND DISCUSSION

We deposited about 0.1-ML H_2Pc molecules on the Fe(001)-whisker substrate at 300 K in UHV and subsequently loaded the sample into the STM. STM/STS measurements were performed at 7 K and 300 K. H_2Pc molecules were observed like a four-leaf clover on the Fe(001) as shown in Fig. 2(a), i.e., H_2Pc single molecules did not "stand" but "lay" on the Fe(001) as hybridized molecular π and Fe(001)

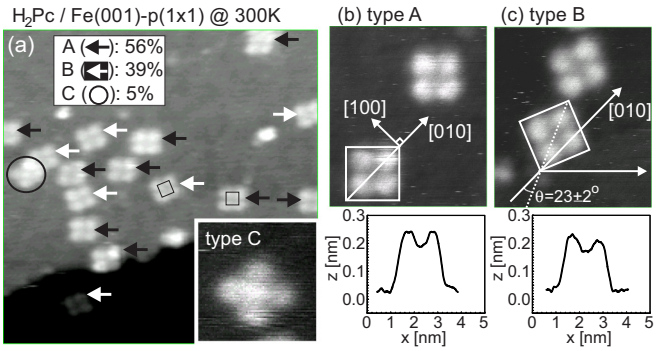

FIG. 2. (a) STM topographic image of the Fe(001) substrate covered by 0.1 ML of H_2Pc molecules ($V_S = -1.0$ V, $I = 50$ pA, 20×20 nm), observed at room temperature. The single molecules are observed. White and black arrows indicate type A and B molecules adsorbing on the bcc Fe(001) with different orientations. Rarely, the molecule marked by the circle was observed: type C. The enlarged image [the inset in (a)] shows a protrusion at the core of the molecule, while there is no protrusion at the core for type A and B molecules. Adsorption probabilities are 56, 39, and 5%, for types A, B, and C, respectively. (b), (c) Enlarged STM topographic images and line profiles of types A and B molecules ($V_S = -1.5$ V, $I = 300$ pA, 5×5 nm).

d states. Each single molecule did not adsorb randomly. They follow to adsorb in particular directions. We confirmed three adsorption types: type A marked by black arrows, B marked by white arrows, and C marked by the circle. Of the adsorbed molecules on Fe(001), 56%, 39%, and 5% are type A, B, and C, respectively, suggesting that the type-A molecules are the most energetically stable.

An enlarged image of the type-A molecules is shown in Fig. 2(b). Single H_2Pc molecules were observed as an assemble of four bright protrusions. Its line profile (at $V_s = -1.5$ V) shows that the molecule has about 200 pm height on Fe(001) and the center is about 50 pm lower. The four bright protrusions are likely four side groups of the H_2Pc. We call the center the "core" and the side groups as "arms." The type-A molecule adsorbed parallel to [010].

The type-B molecules could be the second most stable adsorption site. Its enlarged image is shown in Fig. 2(c). Similar to the type-A molecule, four bright protrusions were observed at about 200 pm height. The type-B molecules adsorb about 23 ± 2 deg out of [010].

Rarely, we observed the type-C molecule. The inset image in Fig. 2(a) shows an enlarged image. Different from type-A and -B molecules, type-C molecule had extra protrusion at the core, i.e., something might exist at the center of the H_2Pc molecule. The type-C molecule tilted about 45 ± 2 deg from [010]. By a chance, there is possibility to enter at the core. Possible candidates are an Fe atom from the substrate, a W atom from the tip, and impurity atoms such as C or O. Thus, the type-C molecules might not be H_2Pc.

We investigated LDOS of the type-A, -B, and -C single molecules observed in Fig. 2 by using STS. Figure 3 shows STS results obtained on the type-A molecule. Figure 3(a) shows dI/dV curves obtained at the core (black circles) and the Fe(001) substrate (gray circles) at 7 K. On the substrate, the sharp peak at +0.17 eV above the Fermi energy (i.e., the minority d states) proves that the observed surface is the bcc Fe(001) substrate [39,41].

Compared to the Fe(001), the dI/dV curve at the core shows peaks around –0.3 eV and +0.2 eV, and also a shoulder around +0.8 eV. These buried LDOS peaks are successfully recovered in the normalized $(dI/dV)/T$ curve by its fitted T function (dotted line). Figure 3(b) shows the obtained $(dI/dV)/T$ curve (black circles). LDOS peaks were investigated by fitting with Gaussian functions. The fitting curve is shown as a black line. Obtained Gaussian peaks are named I, II, III, and IV, having energy positions of peak I -0.22 ± 0.16 eV, peak II $+0.10 \pm 0.05$ eV, peak III $+0.21 \pm 0.11$ eV, and peak IV $+0.53 \pm 0.23$ eV (see Table I).

Next, we performed STS measurements at 300 K, where LDOS peaks are expected to be broadened due to thermal fluctuation. Figure 3(c) shows a $(dI/dV)/T$ curve (black circles) obtained at 300 K with a different tip (tip no. 2). The black line shows an obtained fitting curve by using five Gaussian functions: peak I -0.29 ± 0.18 eV, peak II $+0.14 \pm 0.08$ eV, peak III $+0.29 \pm 0.12$ eV, peak IV $+0.52 \pm 0.18$ eV, and peak V -0.84 ± 0.26 eV. Peaks I–IV exist around the same energy positions as the peaks obtained at 7 K. On the other hand, peak V around -0.85 eV was observed only with tip no. 2; therefore we identify that peak V is a tip state (see Table I).

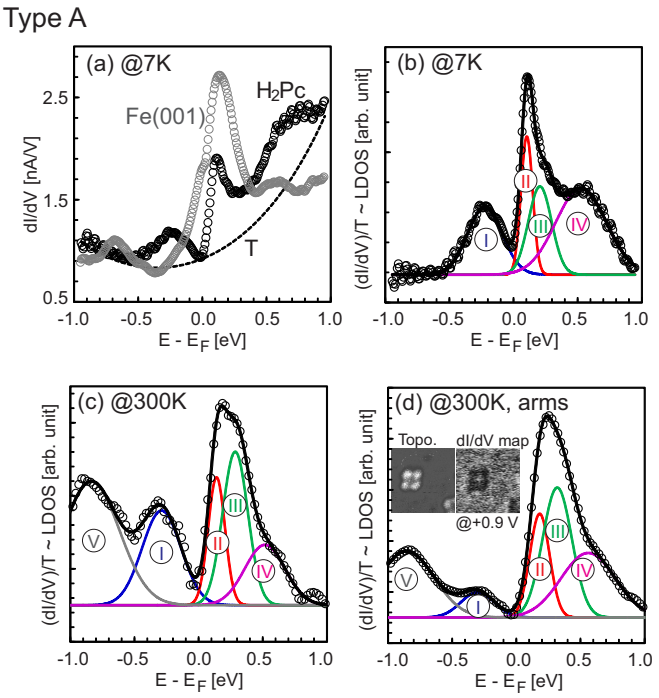

FIG. 3. STS measurements at 7 K and 300 K performed on the single H_2Pc molecules (type A) adsorbed on the Fe(001) whisker. (a) *dI/dV* curves ($V_s = -0.5$ V, $I = 500$ pA) were obtained at 7 K in UHV with tip no.1 on the H_2Pc single molecule (black circles) and the Fe(001) substrate (gray circles). A dotted line denotes a fitted T function. (b) $(dI/dV)/T$ curve (black circles) obtained from the *dI/dV* curve in (a) with the fitted T. The $(dI/dV)/T$ curve was fitted with Gaussian curves. The fitted curve is shown as a black line. Obtained Gaussian peaks were used to determine LDOS peak energy positions labeled I (blue), II (red), III (green), and IV (pink). (c), (d) $(dI/dV)/T$ curve (black circles) obtained on the single H_2Pc molecule at 300 K with a different tip (tip no. 2). The $(dI/dV)/T$ curves were fitted with Gaussian curves. The fitted curves are shown as black lines. Obtained Gaussian peaks were used to determine LDOS peak energy positions labeled I (blue), II (red), III (green), IV (pink), and V (gray), (c) obtained at the core and (d) obtained at the arms. Insets in (d) (5 × 5 nm) show a topographic image and a *dI/dV* map at +0.9 V.

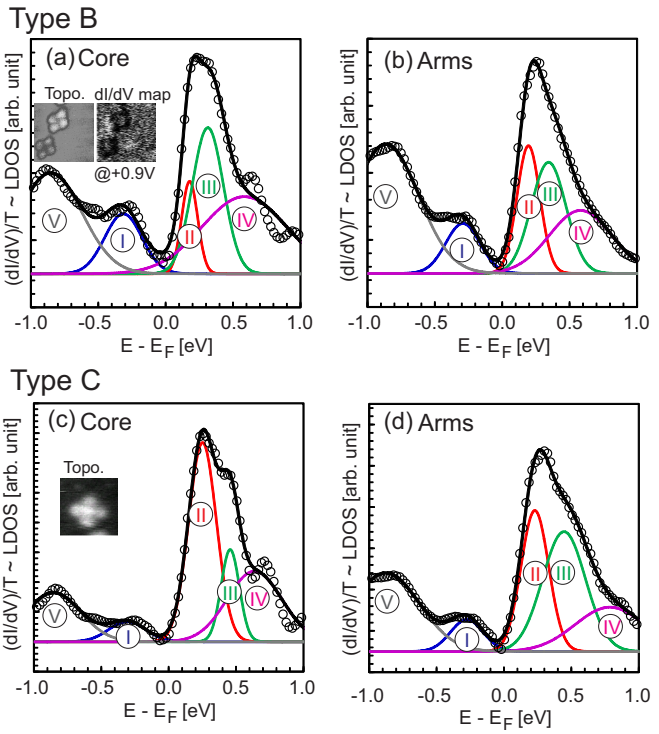

FIG. 4. $(dI/dV)/T$ curve (black circles) measurements at 300 K performed on the type-B and -C single H_2Pc molecules adsorbed on the Fe(001) whisker. The $(dI/dV)/T$ curves were fitted with Gaussian curves. The fitted curves are shown as black lines. Obtained Gaussian peaks were used to determine LDOS peak energy positions labeled I (blue), II (red), III (green), IV (pink), and V (gray). (a), (b) Obtained for the type-B molecule at the core and the arms inside the single molecule, respectively. Insets in (a) (5 × 5 nm) show a topographic image and a *dI/dV* map at +0.9 V. (c), (d) Obtained for a type-C molecule at the core and the arms inside the single molecule, respectively. An inset in (c) (5 × 5 nm) shows a topographic image.

A topographic image and a *dI/dV* map at +0.9 V of the type-A molecule are shown in Fig. 3(d). In the *dI/dV* map, the arms appear darker and the core appears brighter, showing different LDOS exist inside the single molecule. A $(dI/dV)/T$ curve obtained at the arms is shown in Fig. 3(d): peak I -0.30 ± 0.15 eV, peak II $+0.18 \pm 0.09$ eV, peak III $+0.32 \pm 0.13$ eV, and peak IV $+0.56 \pm 0.25$ eV. The core and the arms have the LDOS peaks at the same energy positions, only the amplitude is different. Thus, we experimentally confirmed that the freestanding HOMO/LUMO are significantly influenced by the contact of the molecule with Fe(001) via chemisorption.

In the same way, $(dI/dV)/T$ curves obtained at the type-B molecule are shown in Figs. 4(a) and 4(b). The *dI/dV* map of the type-B molecule in (a) showed the arms appear darker and the core appears brighter, similar to type A, indicating that the core has higher LDOS amplitude. The obtained peak energy

TABLE I. Peak energy positions obtained by Gaussian fittings to the $(dI/dV)/T$ curves experimentally obtained on the core and the arms of the types A, B, and C single H_2Pc molecules on Fe(001). Error bars denote a half-width of half maximum of each Gaussian peak.

Type	Area	Temperature [K]	Tip	Peak I [eV]	Peak II [eV]	Peak III [eV]	Peak IV [eV]	Peak V [eV]
A	Core	7	No. 1	-0.22 ± 0.16	$+0.10 \pm 0.05$	$+0.21 \pm 0.11$	$+0.53 \pm 0.23$	None
A	Core	300	No. 2	-0.29 ± 0.18	$+0.14 \pm 0.08$	$+0.29 \pm 0.12$	$+0.52 \pm 0.18$	-0.84 ± 0.26
A	Arms	300	No. 2	-0.30 ± 0.15	$+0.18 \pm 0.09$	$+0.32 \pm 0.13$	$+0.56 \pm 0.25$	-0.86 ± 0.25
B	Core	300	No. 2	-0.31 ± 0.16	$+0.18 \pm 0.07$	$+0.31 \pm 0.14$	$+0.58 \pm 0.37$	-0.85 ± 0.28
B	Arms	300	No. 2	-0.29 ± 0.15	$+0.19 \pm 0.10$	$+0.34 \pm 0.15$	$+0.58 \pm 0.27$	-0.86 ± 0.28
C	Core	300	No. 2	-0.31 ± 0.16	$+0.25 \pm 0.12$	$+0.45 \pm 0.08$	$+0.64 \pm 0.24$	-0.86 ± 0.24
C	Arms	300	No. 2	-0.28 ± 0.14	$+0.23 \pm 0.12$	$+0.45 \pm 0.19$	$+0.79 \pm 0.30$	-0.88 ± 0.30

positions are peak I -0.31 ± 0.16 eV, peak II $+0.18 \pm 0.07$ eV, peak III $+0.31 \pm 0.14$ eV, and $+0.58 \pm 0.37$ eV for the core, and peak I -0.29 ± 0.15 eV, peak II $+0.19 \pm 0.10$ eV, peak III $+0.34 \pm 0.15$ eV, and peak IV $+0.58 \pm 0.27$ eV for the arms (see Table I). Compared with type A, all the peak energy positions are identical. It is clear that there is no big difference in the LDOS between the type-A and type-B molecules.

Finally, we performed spectroscopy measurements for the type-C molecule. Results are shown in Figs. 4(c) and 4(d). The core likely includes an extra atom. Obtained peak positions are peak I -0.31 ± 0.16 eV, peak II $+0.25 \pm 0.12$ eV, peak III $+0.45 \pm 0.08$ eV, and peak IV $+0.64 \pm 0.24$ eV for the core, and peak I -0.28 ± 0.14 eV, peak II $+0.23 \pm 0.12$ eV, peak III $+0.45 \pm 0.19$ eV, and peak IV $+0.79 \pm 0.30$ eV for the arms

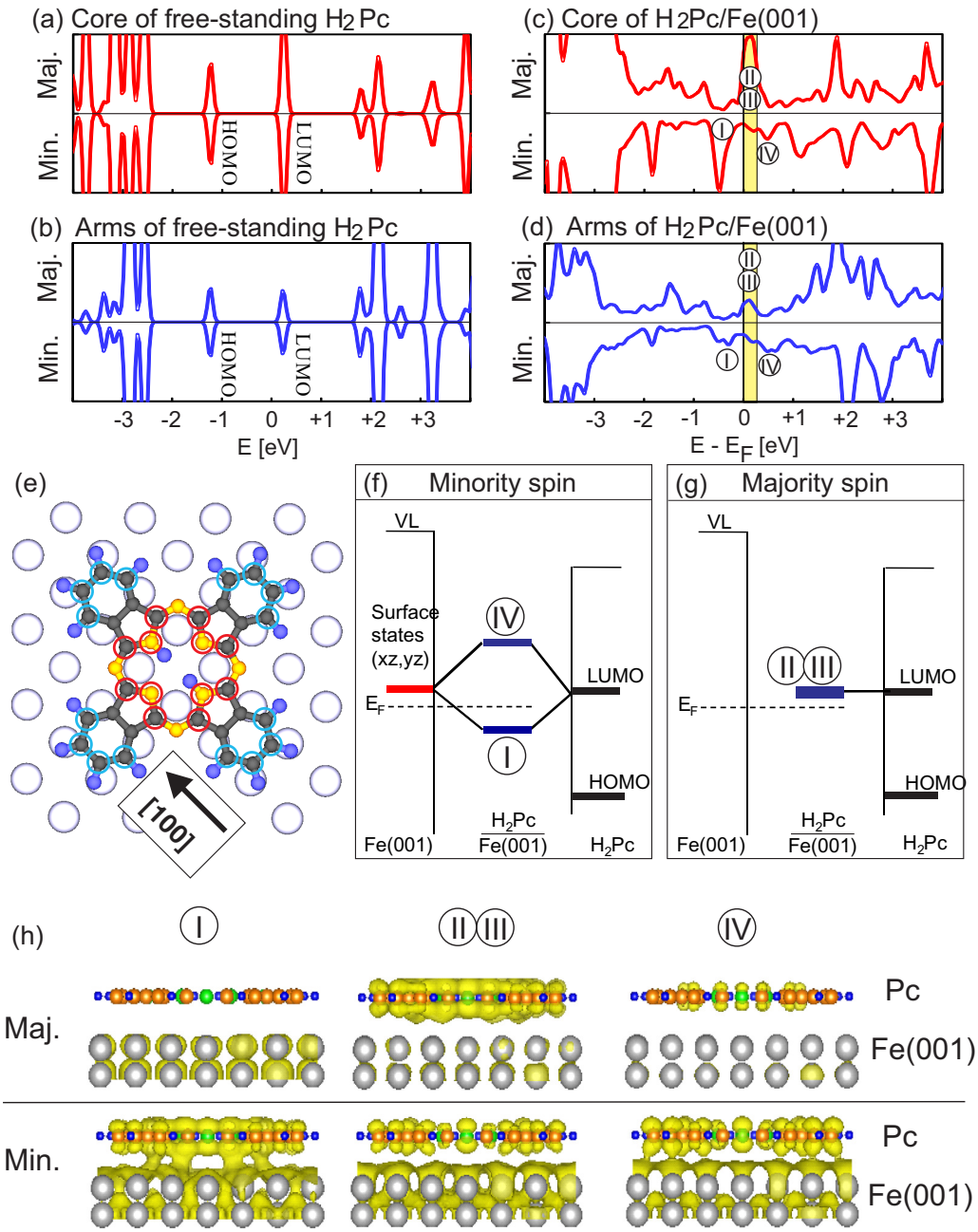

FIG. 5. Calculated spin-resolved LDOS of (a), (b) a freestanding H_2Pc molecule and (c), (d) a single H_2Pc molecule (type A) adsorbed onto bcc Fe(001) substrate. The top and bottom sections show the majority and minority spin states, respectively. I, II, III, and IV denote the energy positions of experimentally determined peaks. (e) Spherical model of a H_2Pc molecule on a square atomic lattice. H (blue sphere), C (gray sphere), and N (yellow sphere) form the constituent chemical species of the molecule. Four nitrogen and eight carbon atoms marked by the red circles are the main contributed atoms for the core. The 16 carbon atoms marked by the blue circles are representatives of the arms. (f), (g) Interface hybridization between H_2Pc and Fe(001) in the minority (f) and the majority (g) spin states. In (f), energy positions of the Fe(001) d_{xz+yz} surface states and the molecular HOMO/LUMO states are shown as red and black lines, respectively. Blue lines denote new hybridized bonding/antibonding states. I and IV denote experimentally obtained peak positions. In (g), there is no peak at the Fe(001) side. No hybridization occurs. (h) Three-dimensional views of minority and majority spin interface states: hybridized molecular π and Fe(001) d states.

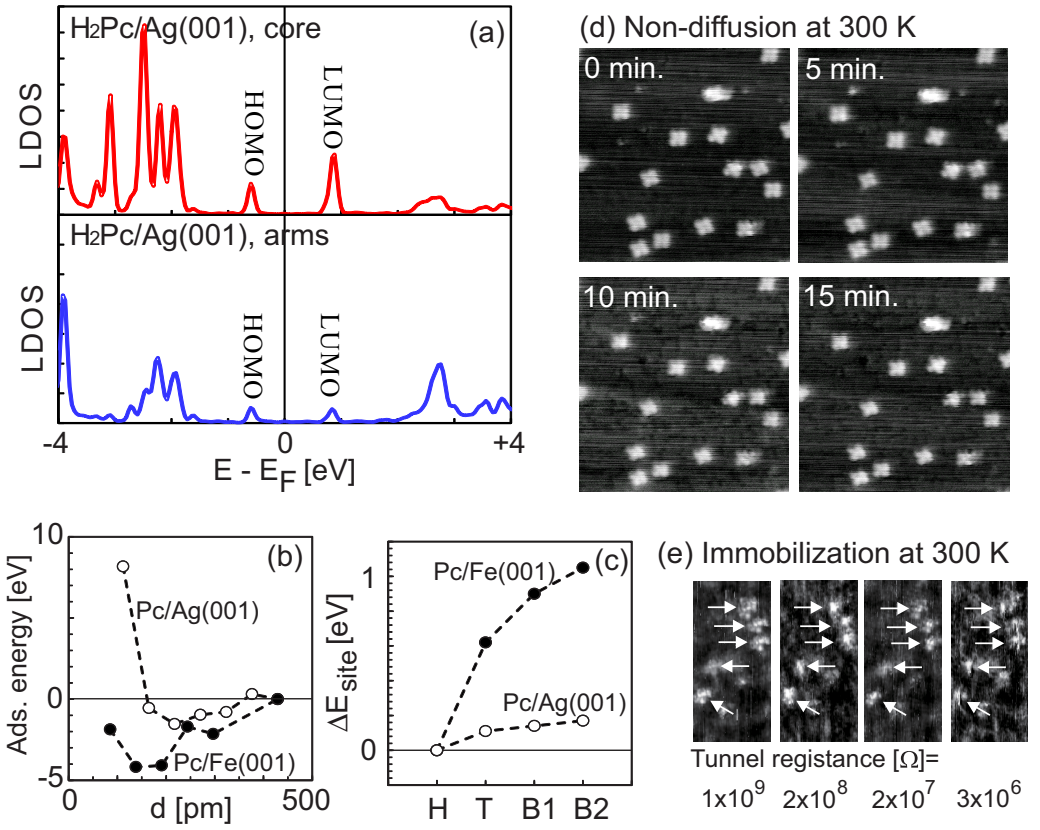

FIG. 6. (a) Calculated LDOS of a single H_2Pc molecule adsorbed onto a fcc Ag(001) substrate. (b) Adsorption energy of a single H_2Pc molecule onto Fe(001) (black dots) and Ag(001) (white dots). The d axis represents the molecule-substrate distance. (c) Energy difference of the diffusion barrier from the fourfold hollow site position (H) for H_2Pc molecules on Ag(001) (white dots) and Fe(001) (black dots). A top site (T), a bridge site along the [010] direction (B1), and a bridge site along the [100] direction (B2) are calculated. (d) Continuous STM images of a given area on which 0.1-ML H_2Pc was adsorbed onto Fe(001) observed at 300 K ($V_s = -600$ mV, $I = 600$ pA, 20×20 nm). The images were sequentially acquired at 5-min intervals. (e) STM images (20×9.4 nm) of this area at different tunneling resistances of 1×10^9 Ohms($V_s = -600$ mV, $I = 600$ pA), 2×10^8 Ohms($V_s = -600$ mV, $I = 3$ nA), 2×10^7 Ohms($V_s = -600$ mV, $I = 30$ nA), and 3×10^6 Ohms($V_s = -100$ mV, $I = 30$ nA). Five single molecules (bright spots) did not move.

(see Table I). Peak I did not change so much from types A and B, while for peaks II, III, and IV, positions shifted clearly. For example, peak III shifted to +0.45 eV from around +0.3 eV for types A and B. The $(dI/dV)/T$ curve suggested that type C could not be H_2Pc.

First-principles calculations were performed to investigate the experimentally found four peaks (I, II, III, and IV) in $(dI/dV)/T$ curves in Fig. 3. Figure 5 shows the calculation results of the energetically stable type-A molecule. Figures 5(a) and 5(b) show a calculated LDOS of a freestanding H_2Pc molecule at the core (a) and the arms (b). HOMO-LUMO states are observed with a gap of about 1.5 eV. Upper and lower panels show majority and minority spin states, respectively. The freestanding H_2Pc is not spin polarized.

Majority and minority spin states of the H_2Pc on Fe(001) were calculated as shown in Figs. 5(c) and 5(d) with the energetically stable configuration in Fig. 5(e) based on experimentally observed configuration in Fig. 2. Adsorption energy at the fourfold hollow site was energetically the most stable [Fig. 6(c)]. In Fig. 5(e), yellow, gray, and blue spheres denote nitrogen, carbon, and hydrogen atoms, respectively. The atoms marked by the red circles belong to the core, and the atoms marked by the blue circles belong to the arms. Figures 5(c) and 5(d) show LDOS at the core and the arms, respectively.

Between majority and minority spin states, a significant difference is observed from −2 eV to +2 eV, i.e., it is spin-polarized. This is not surprising, although so far no report of H_2Pc on Fe(001), phthalocyanine, or porphyrin molecules on Mn(001), Fe(110), and Co(0001) have been reported to be spin-polarized when they contact with 3d magnetic substrates. (So far all reported experiments were performed at low temperatures.)

In Fig. 3, we experimentally found four peaks around the Fermi energy. In the calculated LDOS in Figs. 5(c) and 5(d), we observed three peaks around the Fermi energy. Comparing Figs. 3, 5(c), and 5(d) shows that the origin of peaks II and III is the majority spin states (yellow area), and the peak-I and -IV peaks mainly consist of the minority spin states. Similar to the core, at the arms, the majority spin peak is observed at peaks II and III, and minority spin peaks are observed at peaks I and IV, while the peak amplitude is relatively smaller than the core.

Figures 5(f) and 5(g) show how the non-spin-polarized states of freestanding H_2Pc in Figs. 5(a) and 5(b) change to spin-polarized states when H_2Pc contacts with Fe(001).

The longitudinal axis and horizontal axis denote energy and position, respectively. The molecular minority spin states hybridize with the Fe(001) minority spin states.

Figure 5(f) shows the minority spin states. The left-hand side shows Fe(001) states. As shown in Fig. 3(a), Fe(001) has a strong minority d_{xz+yz} peak above the Fermi energy [the red line in Fig. 5(f)]. In the right-hand side in Fig. 5(f), HOMO/LUMO states of the freestanding H_2Pc are shown as black lines. When the H_2Pc approaches the Fe(001), the Fe(001) minority spin state and H_2Pc LUMO minority spin state are energetically close, and the chemisorption of the H_2Pc arises from the strong hybridization between the LUMO state and the localized state at the Fe surface, which pushes up the bonding and antibonding states in energy where electrons between the H_2Pc and the Fe surface accumulate and deplete, respectively, as illustrated in I and IV in Fig. 5(h). On the other hand, as shown in Fig. 5(g), the Fe(001) does not have the majority spin peak around the Fermi energy. Therefore, the molecular LUMO majority spin state is less affected. As a result, the LUMO majority spin state remains above the Fermi energy.

By following this simple hybridization mechanism, it is speculated that the experimentally observed peaks I and IV are the hybridized minority spin states, and the peaks II and III are the remaining LUMO majority spin state. Indeed, since the peaks II and III, taken on molecules (at 0.14–0.18 eV), are located rather close to the surface states of the Fe(001) substrate (at around 0.17 eV), the spectroscopic features of the substrate may be retained to some extent on the molecule. However, the cross-sectional views of the density distribution of the calculated interface LDOS, as mentioned in Fig. 5(h), may rule out the substrate contribution, since at I and IV, the molecular π and the Fe(001) d states are hybridized, while at II and III, there is no hybridization. Thus, the substrate peaks have no measurable contribution to the molecular peaks, and such a unique hybridization is further supported at the Co(0001) surface experimentally when they contact with π-conjugated phthalocyanine molecules [51].

As already shown in Fig. 2, metal-free H_2Pc molecules were observed as "single" molecules on Fe(001) at 300 K. Spectroscopy measurements were able to be performed stably at 300 K, while such metal-free molecules are known to be diffused on noble metal substrates at 300 K and be formed films [20,24]. Here, we remark that electronic interactions determine the bonding strength between π-conjugated single organic molecules and substrate electrodes, i.e., the insulating electrode exhibits negligible electronic interaction with the substrate. Noble metal surfaces, in which mainly s or p states are dominant near the Fermi energy (E_F), interact weakly with the molecule, essentially through the process of physisorption.

Figure 6(a) shows that the LDOS of H_2Pc molecules adsorbed on Ag(001), which is similar to the freestanding H_2Pc in Figs. 5(a) and 5(b), i.e., the HOMO and LUMO states of the H_2Pc molecule, even after the molecule is adsorbed onto the Ag(001) surface, do not change significantly from those of the freestanding molecule. This leads to weak physisorption, and therefore single H_2Pc molecules easily overcome the diffusion barrier by thermal assistance, even at temperatures less than room temperature.

The interfaces between organic molecules and 3d magnets appear to be spin-polarized, even without the presence of magnetic ions in molecules due to hybridization between the d and π states, and thus, the molecules are likely chemisorbed. Consequently, the distance between the substrate and the molecule is less than that in the physisorption case due to the strong nature of chemisorbed bonds. Such chemisorption may prevent the diffusion of single molecules and generate strong bonding between single molecules and the electrode at 300 K. Adsorption energy when the H_2Pc molecule approaches the Ag(001) and Fe(001) was calculated. Here, Ag(001) was used as the reference for the diffusion case.

The total energy as a function of the molecule-substrate separation (d) for adsorption at the four-fold hollow (H) site was calculated [Fig. 6(b)] under the absence of relaxation for purposes of simplicity. The calculations clearly demonstrate that the adsorption energy on the Fe(001) surface (–4.2 eV at ~0.15 nm) is larger than that of the Ag(001) surface (–1.5 eV at ~0.2 nm) by a factor of about 3. (The adsorption energy difference was assumed to be zero far from the surface at 430 pm.) It is noteworthy that the distances at the energy minimum are approximately equal to the apparent height of the molecules in the STM images, which values are about 0.15 nm and 0.20 nm on the Fe(001) and Ag(001) surfaces, respectively. These theoretical calculations indicate that a single H_2Pc molecule does not diffuse on Fe(001) at 300 K, while H_2Pc on Ag(001) is known to diffuse at 300 K.

To further confirm the robust adsorption of the H_2Pc molecule onto the Fe(001) surface, the total energies at different adsorption sites of the H_2Pc molecule, E_H, E_T, E_{B1}, and E_{B2}, on the Ag(001) and Fe(001) surfaces were calculated, assuming that the center of the molecule locates on the hollow site (H), top site (T), bridge site 1 (B1), and bridge site 2 (B2). In both surfaces, adsorption at the H site is found to be energetically the most favorable. Importantly, the energy differences of the T, B1, and B2 sites with respect to that of the H site, $E_{Site} = E_{Site} - E_H$, indicate that the H_2Pc/Fe(001) system presents a larger energy barrier to thermal diffusion when compared with that of the H_2Pc/Ag(001) system. For the Ag(001) surface, the energy difference is about 0.1–0.2 eV/molecule along the [110], [100], and [010] directions, but for Fe(001), the corresponding values are 0.6, 0.9, and 1.0 eV, which values could thus be sufficiently large to prevent the diffusion of the H_2Pc molecules even at room temperature. By using the Arrhenius equation with the calculated energy barriers, the average time that the molecules spend before diffusing to neighboring sites, e.g., the T sites, is confirmed to be significantly larger on the Fe substrate than that on the Ag substrate by a factor of 10^8 even in a room temperature, where the frequency factor is assumed to be same between the Fe and Ag substrates.

The thermal stability of H_2Pc molecules on Fe(001) was experimentally confirmed by means of consecutively obtained STM images of the same area. Figure 6(d) shows these images, which were sequentially acquired every 5 min. It is obvious that single molecules do not diffuse on Fe(001) at 300 K, which validates the theoretical prediction indicated in Figs. 6(b) and 6(c). The diffusion barrier on Fe(001) needs to be four times that on Ag(001) to prevent diffusion. We attempted to manipulate the single molecules by pushing them along the [110] direction using the STM tip, because this direction has a lower barrier when compared with those of

the [100] and [010] directions [Fig. 6(c)]. The results of our "pushing" are shown in Fig. 6(e). In these cases, we attempted to move five single molecules at different tunneling resistances of $1 \times 10^9\,\Omega$ ($V_s = -600$ mV, $I = 600$ pA), $2 \times 10^8\,\Omega$ ($V_s = -600$ mV, $I = 3$ nA), $2 \times 10^7\,\Omega$ ($V_s = -600$ mV, $I = 30$ nA), and $3 \times 10^6\,\Omega$ ($V_s = -100$ mV, $I = 30$ nA); the molecules did not move in any of the five cases.

Such a robust bonding that cannot be broken by STM tip manipulation indicates the possibility of fabricating room-temperature single-molecule junctions.

IV. CONCLUSIONS

Adsorption and electronic states of metal-free π-conjugated phthalocyanine single molecules adsorbed on the Fe(001)-whisker single crystal were studied by means of UHV-STM and STS at 7 K and 300 K. The single H_2Pc molecules adsorbed with three orientations. Type A is the most energetically stable, parallel to [100], and type B is the second most stable, with a rotation of about 23 deg from [100]. Rarely, type-C molecules are observed with a rotation of about 45 deg from [100]. Type C includes an extra atom at the core, possibly an Fe atom or an impurity atom. Types A and B have similar LDOS peaks. Our *ab initio* calculations nicely recover the experimentally obtained LDOS peaks, suggesting the hybridization process between the molecular LUMO and the Fe(001) d_{xz+yz} states. Since Fe(001) has minority spin states above the Fermi energy, hybridization mainly occurs with the LUMO minority spin states, producing new bonding/antibonding states below/above the Fermi energy. On the other hand, LUMO majority spin states remain without hybridization by the d states; thus spin-polarized LDOS peaks are tailored around the Fermi energy. Further, even inside the same single molecule, core and arms (side groups) have different LDOS and spin polarization, suggesting careful manners to deduce spin polarization of the single molecules using STS. Studies of the H_2Pc single molecules on Fe(001) first theoretically and experimentally verify that systematically we can diffuse or immobilize the π-conjugated single molecules at 300 K by selecting the contacting substrate, which is key knowledge for realization of 300-K single molecular devices. The H_2Pc/Fe(001) system could be the first evidence to prove that the strong π-d bonding can stop molecular diffusion at room temperature.

ACKNOWLEDGMENTS

We thank Dr. D. T. Pierce (NIST) for his guidance regarding the chemical vapor deposition of the Fe whisker. We thank Professor Dr. H. Ishii (Chiba University) and Professor Dr. Y. Noguchi (Meiji University) for supporting purification of the molecules, Professor Dr. F. Shibahara (Gifu University) for NMR and IR measurements, and R. Nemoto for the Gaussian fittings. Computations were performed at the Supercomputer Center, Institute for Solid State Physics, University of Tokyo, Center for Computational Materials Science, Institute for Materials Research, Tohoku University, and Research Institute for Information Technology, Kyushu University. This work was supported by JSPS KAKENHI Grants No. 23681018 and No. 25110011, the Japan Science and Technology Agency (JST) – Improvement of Research Environment for Young Researchers, Chiba University Young Research – Oriented Faculty Member Development Program in Bioscience Areas, Casio Science Promotion Foundation, Asahi Glass Foundation, Hatakeyama Culture Foundation, The Association for the Progress of New Chemistry, Iketani Science and Technology Foundation, The Noguchi Institute, Ozawa Yoshikawa Memorial Electronics Foundation, Research Foundation for the Electrotechnology of Chubu, The Nakajima Foundation, The Futaba Electronics Memorial Foundation, and Shimadzu Foundation.

[1] A. C. Ferrari and D. M. Basko, Nat. Nanotechnol. **8**, 235 (2013).
[2] S. Z. Butler, S. M. Hollen, L. Cao, Y. Cui, J. A. Gupta, H. R. Gutiérrez, T. F. Heinz, S. S. Hong, J. Huang, A. F. Ismach *et al.*, ACS Nano **7**, 2898 (2013).
[3] S. Park, M. Vosguerichian, and Z. A. Bao, Nanoscale **5**, 1727 (2013).
[4] Q. Zhang, J. Q. Huang, W. Z. Qian, Y. Y. Zhang, and F. Wei, Small **9**, 1237 (2013).
[5] U. N. Maiti, W. J. Lee, J. M. Lee, Y. Oh, J. Y. Kim, J. E. Kim, J. Shim, T. H. Han, and S. O. Kim, Adv. Mater. **26**, 40 (2014).
[6] Y. Zang, C. Z. Li, C. C. Chueh, S. T. Williams, W. Jiang, Z. H. Wang, J. S. Yu, and A. K. Y. Jen, Adv. Mater. **26**, 5708 (2014).
[7] Y. H. Zhou, J. Zeng, L. M. Tang, K. Q. Chen, and W. P. Hu, Org. Electron. **14**, 2940 (2013).
[8] B. O. Jahn, H. Ottosson, M. Galperin, and J. Fransson, ACS Nano **7**, 1064 (2013).
[9] L. Gross, F. Mohn, N. Moll, P. Liljeroth, and G. Meyer, Science **325**, 1110 (2009).
[10] H. J. Shin, J. Jung, K. Motobayashi, S. Yanagisawa, Y. Morikawa, Y. Kim, and M. Kawai, Nat. Mater. **9**, 442 (2010).
[11] T. Miyamachi, M. Gruber, V. Davesne, M. Bowen, S. Boukari, F. Scheurer, G. Rogez, T. K. Yamada, P. Phresser, E. Beaurepaire, and W. Wulfhekel, Nat. Commun. **3**, 938 (2012).
[12] G. Schull, T. Frederiksen, M. Brandbyge, and R. Berndt, Phys. Rev. Lett. **103**, 206803 (2009).
[13] J. Brede, N. Atodiresei, S. Kuck, P. Lazić, V. Caciuc, Y. Morikawa, G. Hoffmann, S. Blügel, and R. Wiesendanger, Phys. Rev. Lett. **105**, 047204 (2010).
[14] S. Schmaus, A. Bagrets, Y. Nahas, T. K. Yamada, A. Bork, F. Evers, and W. Wulfhekel, Nat. Nanotechnol. **6**, 185 (2011).
[15] S. L. Kawahara, J. Lagoute, V. Repain, C. Chacon, Y. Girard, S. Rousset, A. Smogunov, and C. Barreteau, Nano Lett. **12**, 4558 (2012).
[16] A. Bagrets, S. Schmaus, A. Jaafar, D. Kramczynski, T. K. Yamada, M. Alouani, W. Wulfhekel, and F. Evers, Nano Lett. **12**, 5131 (2012).
[17] M. Mannini, F. Pineider, P. Sainctavit, C. Danieli, E. Otero, C. Sciancalepore, A. M. Talarico, M.-A. Arrio, A. Cornia, D. Gatteschi, and R. Sessoli, Nat. Mater. **8**, 194 (2009).

[18] M. Mannini, F. Pineider, P. Sainctavit, L. Joly, A. Fraile-Rodriguez, M.-A. Arrio, C. C. Moulin, W. Wernsdorfer, A. Cornia, D. Gatteschi, and R. Sessoli, Adv. Mater. **21**, 167 (2009).
[19] L. Bogani and W. Wernsdorfer, Nat. Mater. **7**, 179 (2008).
[20] N. Tsukahara, K.-i. Noto, M. Ohara, S. Shiraki, N. Takagi, Y. Takata, J. Miyawaki, M. Taguchi, A. Chainani, S. Shin, and M. Kawai, Phys. Rev. Lett. **102**, 167203 (2009).
[21] T. Komeda, H. Isshiki, J. Liu, Y. F. Zhang, N. Lorente, K. Katoh, B. K. Breedlove, and M. Yamashita, Nat. Commun. **2**, 217 (2010).
[22] I. Chizhov, G. Scoles, and A. Kahn, Langmuir **16**, 4358 (2000).
[23] A. Scarfato, S. H. Chang, S. Kuck, J. Brede, G. Hoffmann, and R. Wiesendaner, Surf. Sci. **602**, 677 (2008).
[24] Y. Yamagishi, S. Nakashima, K. Oiso, and T. K. Yamada, Nanotechnology **24**, 395704 (2013).
[25] A. Zhao, Q. Li, L. Chen, H. Xiang, W. Wang, S. Pan, B. Wang, X. Xiao, J. Yang, J. G. Hou, and Q. Zhu, Science **309**, 1542 (2005).
[26] T. A. Jung, R. R. Schlittler, J. K. Gimzewski, H. Tang, and C. Joachim, Science **271**, 181 (1996).
[27] S. J. H. Griessl, M. Lackinger, F. Jamitzky, T. Markert, M. Hietschold, and W. M. Heckl, J. Phys. Chem. **108**, 11556 (2004).
[28] P. A. Sloan and R. E. Palmer, Nature (London) **434**, 367 (2005).
[29] H. Yang, A. J. Mayne, G. Comtet, G. Dujardin, Y. Kuk, S. Nagarajan, and A. Gourdon, Phys. Rev. B **90**, 125427 (2014).
[30] C. Waeckerlin, K. Tarafder, J. Girovsky, J. Nowakowski, T. Háhlen, A. Shchyrba, D. Siewert, A. Kleibert, F. Nolting, P. M. Oppeneer *et al.*, Angew. Chem. Int. Ed. **52**, 4568 (2013).
[31] H. C. Herper, M. Bernien, S. Bhandary, C. F. Hermanns, A. Krüger, J. Miguel, C. Weis, C. Schmitz-Antoniak, B. Krumme, D. Bovenschen, *et al.*, Phys. Rev. B **87**, 174425 (2013).
[32] T. Konishi, M. Kiguchi, M. Takase, F. Nagasawa, H. Nabika, K. Ikeda, K. Uosaki, K. Ueno, H. Misawa, and K. Murakoshi, J. Am. Chem. Soc. **135**, 1009 (2013).
[33] D. Xiang, H. Jeong, D. Kim, T. Lee, Y. Cheng, Q. Wang, and D. Mayer, Nano Lett. **13**, 2809 (2013).
[34] M. L. Perrin, R. Frisenda, M. Koole, J. S. Seldenthuis, J. A. C. Gil, H. Valkenier, J. C. Hummelen, N. Renaud, F. C. Grozema, J. M. Thijssen *et al.*, Nat. Nanotechnol. **9**, 830 (2014).
[35] Z. Li and E. Borguet, J. Am. Chem. Soc. **134**, 63 (2012).
[36] M. Kiguchi, S. Nakashima, T. Tada, S. Watanabe, S. Tsuda, Y. Tsuji, and J. Terao, Small **8**, 726 (2012).
[37] K. Kaasbjerg and K. Flensberg, Phys. Rev. B **84**, 115457 (2011).
[38] V. A. Sydoruk, D. Xiang, S. A. Vitusevich, M. V. Petrychuk, A. Vladyka, Y. Zhang, A. Offenhäusser, V. A. Kochelap, A. E. Belyaev, and D. Mayer, J. Appl. Phys. **112**, 014908 (2012).
[39] J. A. Stroscio, D. T. Pierce, A. Davies, R. J. Celotta, and M. Weinert, Phys. Rev. Lett. **75**, 2960 (1995).
[40] J. Unguris, R. J. Celotta, and D. T. Pierce, Phys. Rev. Lett. **79**, 2734 (1997).
[41] M. M. J. Bischoff, T. K. Yamada, C. M. Fang, R. A. de Groot, and H. van Kempen, Phys. Rev. B **68**, 045422 (2003).
[42] V. A. Ukraintsev, Phys. Rev. B **53**, 11176 (1996).
[43] T. K. Yamada, M. M. J. Bischoff, T. Mizoguchi, and H. van Kempen, Surf. Sci. **516**, 179 (2002).
[44] T. K. Yamada, M. M. J. Bischoff, G. M. M. Heijnen, T. Mizoguchi, and H. van Kempen, Phys. Rev. Lett. **90**, 056803 (2003).
[45] L. Gerhard, T. K. Yamada, T. Balashov, A. F. Takacs, R. J. H. Wesselink, M. Daene, M. Fechner, S. Ostanin, A. Ernst, I. Mertig, and W. Wulfhekel, Nat. Nanotechnol. **5**, 792 (2010).
[46] T. K. Yamada, T. Abe, N. M. K. Nazriq, and T. Irisawa, Rev. Sci. Instrum. **87**, 033703 (2016).
[47] J. P. Perdew, K. Burke, and M. Ernzerhof, Phys. Rev. Lett. **77**, 3865 (1996).
[48] E. Wimmer, H. Krakauer, M. Weinert, and A. J. Freeman, Phys. Rev. B **24**, 864 (1981).
[49] M. Weinert, E. Wimmer, and A. J. Freeman, Phys. Rev. B **26**, 4571 (1982).
[50] K. Nakamura, T. Ito, A. J. Freeman, L. Zhong, and J. Fernandez-de-Castro, Phys. Rev. B **67**, 014420 (2003).
[51] C. Iacovita, M. V. Rastei, B. W. Heinrich, T. Brumme, J. Kortus, L. Limot, and J. P. Bucher, Phys. Rev. Lett. **101**, 116602 (2008).